CHAPTER 3

Instrumentation & Characterisation

3.1 Introduction

This chapter deals with the principles of the main analytical techniques used in this study which includes:

- Ultraviolet-visible (UV-VIS) spectroscopy
- Attenuated total reflectance Fourier Transform Infrared spectroscopy (ATR-FTIR)
- X-ray photoelectron (XPS) spectroscopy
- X-ray diffraction (XRD) analysis
- Electron spin resonance (ESR) spectroscopy
- Scanning electron microscopy (SEM)
- Contact angle measurements
- Differential scanning calorimetry (DSC)
- Dynamic mechanical testing

The parameters and experimental conditions used for each instrument will be described in the relevant sections (refer to **Chapters 4-5**).

3.2 Chemical characterisation

In this study spectroscopic analyses were used to study the chemical properties of the PNIPAAm scaffolds. Spectroscopy refers to the study of matter and its interaction with electromagnetic radiation. The electromagnetic spectrum is the range of all possible electromagnetic radiation which is comprised of gamma rays, X-rays; ultraviolet; visible; infra-red; microwave; and radio waves (**Figure 3.1**). The electromagnetic spectrum of a molecule or object will display the characteristic radiation either absorbed or emitted by that particular molecule. Electromagnetic waves are typically expressed by three physical properties i.e. frequency, wavelength or photon energy as expressed in **Equation 3.1**.

$$E = h\nu\,,\ \text{where}\ \nu = c/\lambda \qquad \text{(Eq 3.1)}$$

Where E is the photon energy, h is planks constant, ν is the frequency, c is the speed of light in a vacuum, and λ is the wavelength of light.

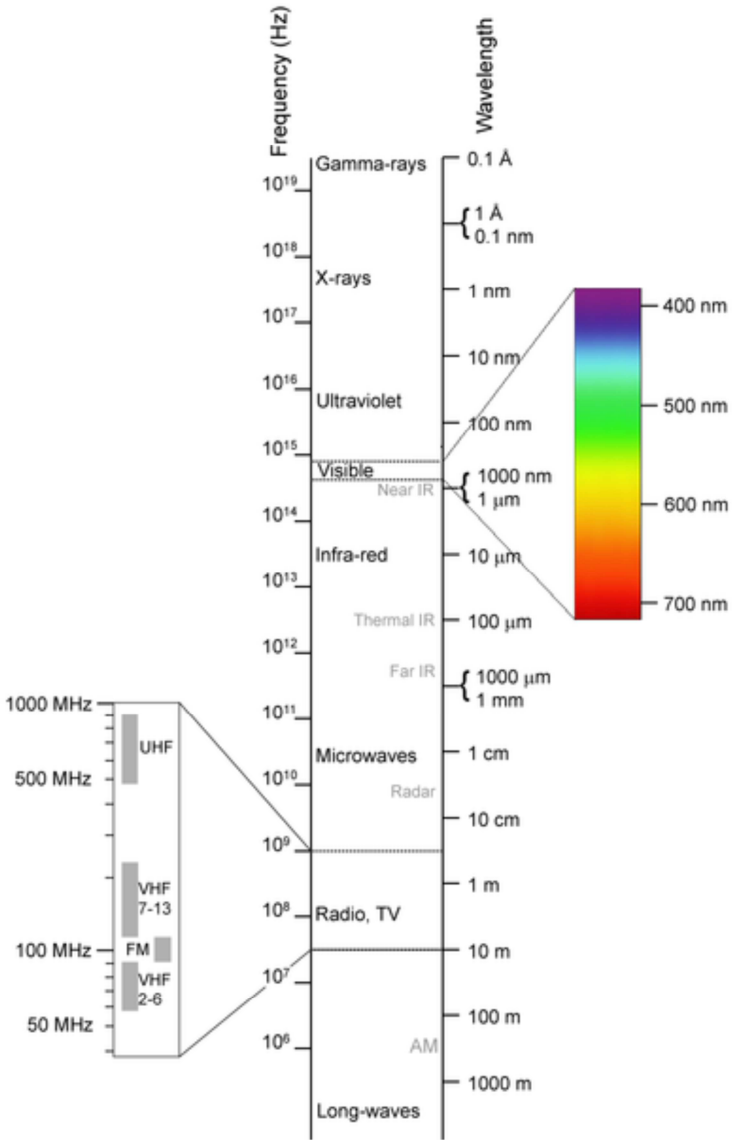

Figure 3.1: Electromagnetic spectrum (Wikipedia, 2012a).

The wavenumber (cm^{-1}) is inversely proportional to wavelength. Gamma rays occur at shortest wavelength and display the highest energy. In this study, infra-red, ultraviolet-visible, X-rays, and microwaves have been used to study the chemical structure of the PNIPAAm scaffolds.

3.2.1 UV-VIS

Ultraviolet-visible (UV-VIS) spectroscopy measures the absorption of materials in the UV-VIS region (180-800 nm). Every molecule possesses a unique series of closely spaced energy levels, the lowest of which is known as the ground state. When a photon of radiation passes near a molecule with energy equal to the energy difference between the ground state and a higher electronic state, the energy of the

photon is absorbed by the molecule as shown in **Equation 3.2**. This results in an energy transfer from the ground state to the higher excited energy state as follows;

$$M + h\nu \longrightarrow M^{*} \qquad \text{(Eq. 3.2)}$$

Whereby a species M is converted to its excited state M^{*} by the absorption of a photon hν. These transitions are responsible for the UV-visible spectra observed for molecules. This process of absorption occurs in a brief period (10^{-6} – 10^{-9} seconds) and is specific to a characteristic molecule (Skoog et al., 1996).

The basic spectrophotometer consists of five main components. These include an energy source, a monochromator, a sample cell (and reference cell), a detector and a readout device (**Figure 3.2**). Radiation from the source first passes to the monochromator, which consists of gratings or prisms that permits isolation of a specific wavelength region. The monochromatic beam is then split into two, one passing through the absorbing sample, while the other passes through a reference cell. The reference cell contains the blank, which is essentially the solvent that has no analyte element. The difference between the two signals is determined electronically and displayed on a screen by the readout device.

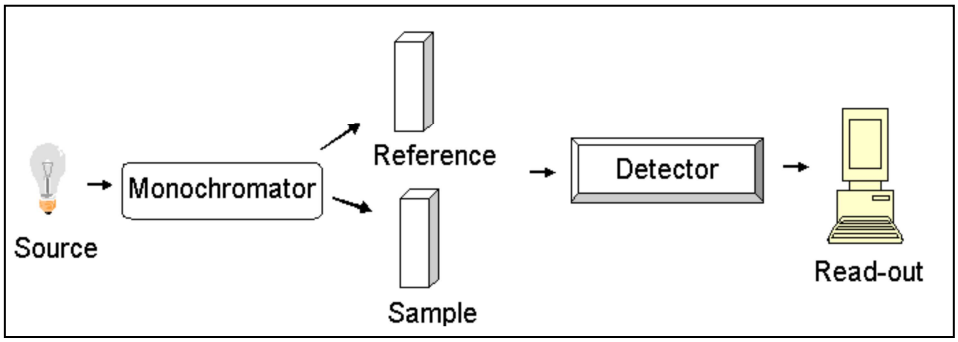

Figure 3.2: Schematic diagram of a typical absorption spectrometer.

Absorption of the analyte can be related to the concentration by the Beer-Lamberts law given by **Equation 3.3** (Skoog et al., 1996):

$$A = \varepsilon bc \qquad \text{(Eq. 3.3)}$$

Where A is absorbance, ε is the absorptivity, b is the path-length through the medium; and c is the concentration. Electrons which are easily excited by UV-VIS radiation involve those that are localised around atoms such as oxygen; sulphur; nitrogen; and halogens (Skoog et al., 1996). Some of the functional groups which typically absorb in the UV-VIS region include aromatic rings, double and triple bonds (C=C, C=O, COOH; N=N), and saturated organic compounds containing heteroatoms (incl. alcohols, ethers, halogenated compounds etc.).

3.2.2 ATR-FTIR

Fourier transform infrared (FTIR) spectroscopy is used to measure the vibration of a molecule which is a unique physical property of a molecule (Coates, 2000). IR occurs between the visible and microwave radiation. IR waves spans from the near-IR (13 000-4000 cm^{-1}); mid-IR (4000-400 cm^{-1}) and far-IR (400-10 cm^{-1}). The mid-IR region is typically used for FTIR spectroscopy. Since molecules have bonds that are continuously moving, bond vibrations can occur on adsorption of IR which include stretching (symmetric or asymmetric), and bending. In this study attenuated total reflectance Fourier transform infrared (ATR-FTIR) spectroscopy was used, which is based on internal reflectance enabling surface analysis of samples.

IR spectra is a fingerprint for identification of molecules since specific structural features in a molecule produce reproducible and characteristic adsorption spectra (Coates, 2000). The fundamental requirement for infrared activity, is that there must be a net change in dipole moment during the vibration (Coates, 2000). Hence highly polar groups (e.g. O-H, N-H) produce strong peaks in the IR region. The vibrational frequency of a molecule is given by Hookes law by **Equation 3.4**:

$$\nu = \frac{1}{2\pi c}\sqrt{k/\mu} \qquad \text{(Eq. 3.4)}$$

Where ν is the fundamental vibration frequency; k is the force constant, μ is the reduced mass which is given as $\mu = m_1 * m_2/(m_1+m_2)$,where m_1 and m_2 are the component masses for the chemical bond under consideration (Coates, 2000). Hence it stands to reason that the higher the bond strength between two atoms the higher the frequency of absorption (i.e. absorption occurs at higher wavenumbers), while the larger the masses of the atoms contained in the bond, the smaller is the wavenumber of absorption. However other factors also contribute to the vibrational

frequencies of bonds such as attraction and repulsion of the electron cloud, the bond length etc., which is not accounted for above. The adsorption intensity is dependent on the electronegativity difference between the atoms in the bond, and the number of specific bonds present.

In the FTIR technique, a polychromatic light source is used (containing light of various wavelengths) which is collimated and directed to a beam-splitter. About 50% of the light is reflected towards the fixed mirror and 50% is transmitted towards the moving mirror, after which the beams recombine to create an interferogram, and 50% of the original light then passes into the sample compartment. ATR-FTIR (**Figure 3.3**) operates by using an ATR crystal onto which the sample is placed, and the technique measures the changes that occur in a totally internally reflected infrared beam when the beam comes into contact with a sample.

Figure 3.3: Image showing an ATR-FTIR instrument.

In the ATR-FTIR technique, a beam of IR light passes through the crystal such that the light reflects of the internal surface of the crystal which is in contact with the sample (**Figure 3.4**). This creates an evanescent wave which then extends into the sample surface. The penetration depth into the sample is typically between 0.5-2 µm and hence surface analysis is possible. An ATR crystal displays a high refractive index and typically includes germanium, zinc selenide, silicon, and diamond. The ATR-FTIR offers an advantage in that solid and liquid samples can be analysed directly without any preparation. The sample absorbs all the different wavelengths characteristic to its spectrum, and the emitted light is then directed to the detector

which measures variation in energy with time at the different wavelengths. A mathematical model called a Fourier Transform is used to convert the raw data into intensity vs. wavelength.

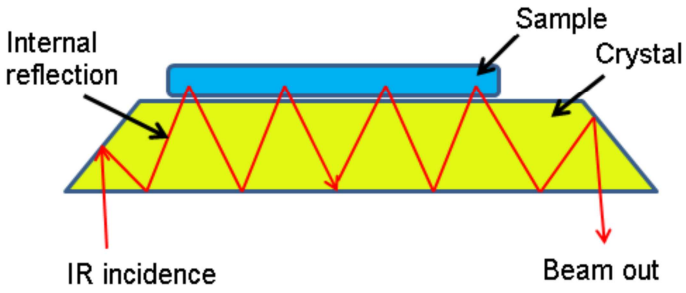

Figure 3.4: Schematic showing working principle of ATR-FTIR.

3.2.3 XPS

X-ray photoelectron spectroscopy (XPS) is used to determine the elemental composition of solid surfaces. During XPS analysis, a sample is placed in an ultrahigh vacuum, and the surface is irradiated with an X-ray source producing photons of a specific energy. Either Al Ka (1486.6 eV) or Mg Ka (1253.6 eV) x-ray sources are used (Torres, 2006). The X-ray photons penetrate the sample to a micrometer depth, hitting the core-1s electrons of the atoms which then emit a core electron leaving an electron vacancy (**Figure 3.5**). A cylindrical mirror analyzer is used to measure the kinetic energy of the emitted electrons.

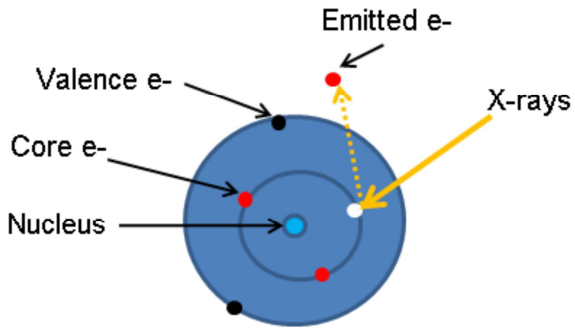

Figure 3.5: Schematic showing interaction between X-rays and an atom during XPS analysis.

The binding energy is determined as given in **Equation 3.5**.

$$KE = hv - BE - \emptyset \quad \text{(Eq 3.5)}$$

Where KE and BE is the kinetic and binding energies respectively, hν is the photon energy from the X-ray source; and ∅ is the spectrometer work function which is found by calibration.

The binding energies of the emitted electrons are plotted and the elements are identified from their binding energy peak positions. Photoelectrons are emitted from a depth of a few nanometers enabling surface analysis of materials. XPS of most elements can be measured with the exception of H_{1s} and He_{1s} where their diatomic mass is too small to enable release of core shell electrons.

3.2.4 XRD

X-ray diffraction (XRD) is a technique used to determine the chemical and crystallographic properties of solids. Solid matter is generally classified as either amorphous or crystalline (or semi-crystalline). In an amorphous material atoms are arranged randomly, while in a crystalline material atoms display a well ordered regular 3D structure.

During X-ray diffraction, electrons from a cathode are accelerated under high voltages (45-50 kV) and strike a metal anode surface which generates X-rays. Copper metal is commonly used as the anode material, and was also used in this study. When the generated X-rays impinge on the solid sample, the X-rays are scattered by the electrons contained in the atoms of the crystal lattice. The scattered X-rays produce secondary spherical waves known as elastic scattering which undergo destructive interference. However if the atoms are arranged symmetrically, the secondary waves add constructively in a few specific directions determined by Braggs law (**Figure 3.6**).

According to Braggs law, the X-rays scattered from adjacent planes will combine constructively only when the angle θ between the plane and the X-ray results in a path-length difference (2 d sinθ) that is equal to an integer multiple of the X-ray wavelength as shown in **Equation 3.6** (Wikipedia, 2012d).

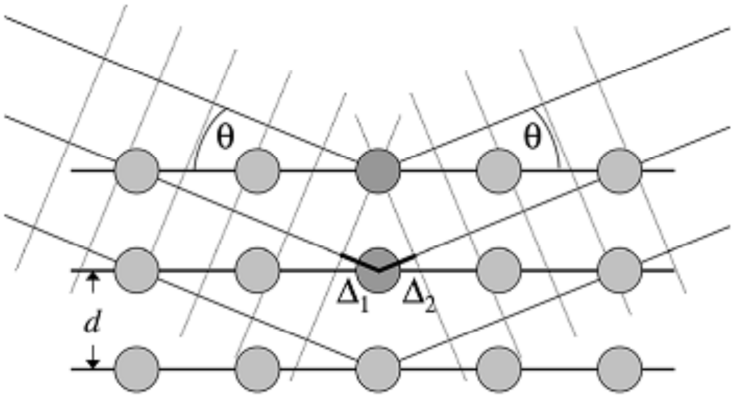

Figure 3.6: Principle of Braggs law for X-ray diffraction (Birkholz, 2006).

This causes the incoming beam to be deflected which produces a diffraction pattern.

$$n\lambda = 2d\sin\theta \qquad \text{(Eq 3.6)}$$

Where d is the spacing between diffracting planes, θ is the incident angle, n is any integer, and λ is the wavelength of the beam (Wikipedia, 2012d). X-rays are used to produce a diffraction pattern since the monochromatic wavelength is typically of the same magnitude (0.1-10 nm) as the d-spacing in the crystal lattice (Wikipedia, 2012d).

The diffraction pattern is due to the specific d-spacing in the crystalline solid, and since the d-spacing pattern is unique for every crystalline solid, the diffraction pattern produces a finger-print for the specific solid. Due to the regular periodic structures in crystalline solids, strong signals are observed whose intensity increases with an increase in the crystal plane electrons (Wikipedia, 2012d). Amorphous structures on the other hand have reduced signal intensities due to the random orientation. Less crystalline structures are detected by a broadening in the peak bands.

When the sample is placed at a short distance from the detector the diffraction maxima appear at $\theta > 5°$ and the XRD technique is referred to as wide angle X-ray scattering (WAXS). Alternatively for small-angle X-ray scattering (SAXS), the distance between the sample and the detector is larger and thus diffraction maxima occur at smaller angles with θ close to zero (Wikipedia, 2012e).

3.2.5 ESR

Electron spin resonance (ESR) which is also known as electron paramagnetic resonance is a technique used to study the interaction of an external magnetic field with an unpaired electron in a species (Bovet, 2009). ESR is an important tool which is commonly used for investigating free radicals formed in solid materials.

ESR is based on the fact that electrons are charged particles which display a spin. When an unpaired electron is placed in a magnetic field, the spin state of the electron is lifted, creating two spin states i.e. m_s = +1/2) or m_s = -1/2, whereby the latter represents the lower energy field which is aligned with the magnetic field (**Figure.3.7**).

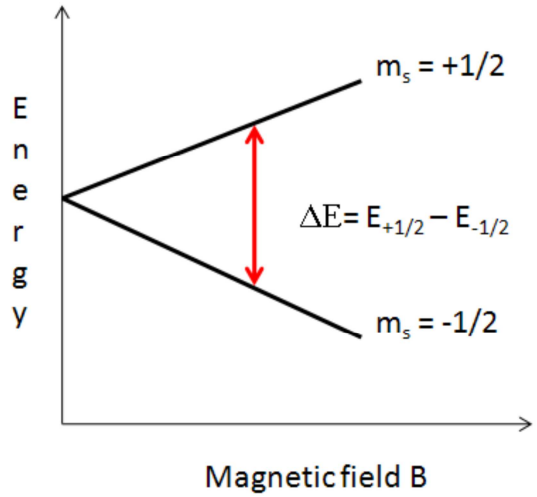

Figure 3.7: Schematic of a single electron spin during the presence of an external magnetic field.

However when electromagnetic radiation in the microwave range is applied spin transitions can occur between the two spin states (Bovet, 2009). The energy difference between the two states (ΔE) is given by **Equation 3.7** (Bovet, 2009):

$$\Delta E = E_{+} - E_{-} = g\beta B = h\nu \qquad \text{(Eq 3.7)}$$

Where β is the Bohr magneton (9.274 x 10^{-24} J T^{-1}), B is the strength of the magnetic field in Tesla, g is known as the g-factor, h is Planck's constant (6.626 x 10^{-34} J s^{-1}),

and ν is the frequency of radiation. The g-factor refers to the intrinsic magnetic moment of the electron, and the g-factor for a free electron is 2.0023 (Bovet, 2009).

When microwave radiation is applied at a frequency corresponding to ΔE, resonance occurs i.e. absorption of the electromagnetic radiation occurs, which is the principle of ESR (Simovič, 2004). ESR spectra are generally presented as the first derivative of the absorption spectra for ease of interpretation (Bovet, 2009).

3.3 SEM

Scanning electron microscopy (SEM) enables observation and characterisation of materials in 3D on a micrometer to nanometer scale. The resolution of a SEM ranges from 1-20 nm, enabling very small features to be detected which are not possible by a light microscope or the naked eye. SEM uses electrons to form a virtual image of a sample rather than a real image which is the case with an optical microscope.

The main component of a SEM is the electron gun which is located at the top of the electron column, a sample chamber which is operated under vacuum, a detector, and a viewing system (**Figure 3.8**) (Philips Electron Optics, 1996).

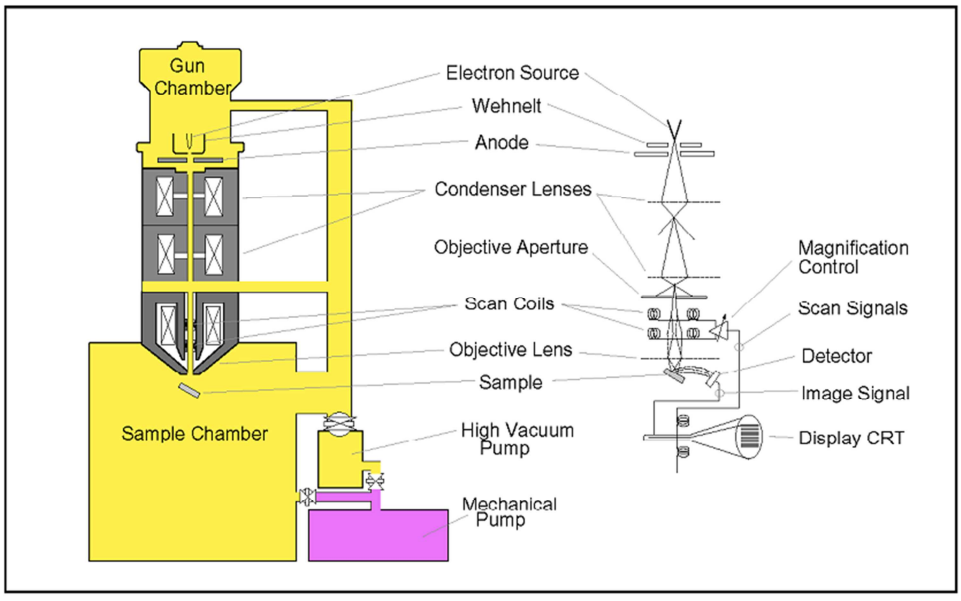

Figure 3.8 : Schematic representation of a SEM (Philips Electron Optics, 1996).

The basic principal of operation includes the following: an electron beam is generated by the electron gun which is accelerated in the electron column at high voltages, and

focused onto the sample surface. The beam is deflected in a scanning pattern over the sample, and interaction between the electron beam with atoms at or near the sample surface generates a variety of signals including: secondary electrons, back-scattered electrons, characteristic X-rays, etc. (Philips Electron Optics, 1996). Various detectors are available for detection of the different signals. Secondary electrons are of very low energy (<50 eV), and escape from the outermost surface of a sample, thereby offering the best imaging resolution (Philips Electron Optics, 1996). X-rays may also be detected in a SEM equipped with energy-dispersive X-ray spectroscopy which enables both qualitative and quantitative data to be obtained regarding the surface elemental composition (Wikipedia, 2012b).

For SEM analysis, samples must be electrically conducting to prevent the accumulation of electric charge at the surface. Metals are therefore easily imaged using SEM without requiring special preparation. However non-conducting materials (such as most polymers) tend to charge when scanned by the electron beams making imaging difficult. Non-conducting material are normally coated with an ultrathin layer of an electrically conducting material (such as gold, palladium, tungsten or graphite,) by sputter-coating prior to imaging.

While the conventional SEM offer many advantages over optical microscopy some of the constraints include the use of a high vacuum, conductive coating on material which can hide small surface features, as well as the need for drying samples prior to imaging. Biological samples are normally fixated in glutaraldehyde prior to imaging.

An advancement to the conventional SEM is the Environmental SEM (ESEM) which allows wet samples to be imaged under low vacuum by the use of a secondary-electron detector(Wikipedia, 2012b). ESEM is particularly attractive for biological and non-metallic samples, since no sample preparation is required.

3.4 Contact Angle

The contact angle of a liquid on a solid surface is a very useful property to quantify wetting, hydrophilicity, and to determine the interfacial free energy of a material. Contact angle is conventionally measured using a contact angle goniometer (**Figure 3.9**), and it is determined as the angle at which the liquid/vapour interface meets the solid surface.

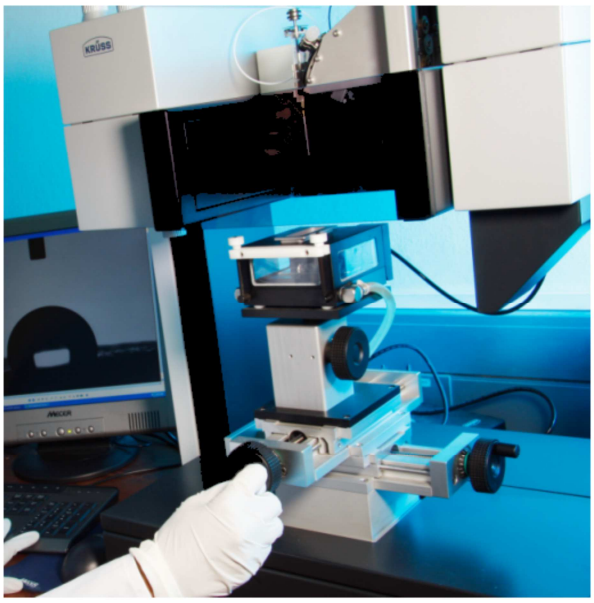

Figure 3.9: Image showing a contact angle goniometer.

The shape of a liquid/vapour interface can be determined by the Young-Laplace equation given by **Equation 3.8** (Goss, 2010):

$$\mathrm{Cos}\theta = \frac{\sigma_{SV} - \sigma_{SL}}{\sigma_{LV}} \qquad \text{(Eq. 3.8)}$$

Where $\sigma_{SV,}$ $\sigma_{SL,}$ and σ_{LV} are the interfacial surface tensions between solid and vapour, solid and liquid and liquid and vapour respectively (**Figure 3.10**).

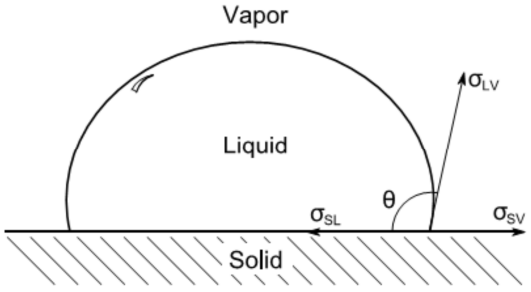

Figure 3.10: Contact angle measurement on a solid surface (Goss, 2010).

If the contact angle is small, a drop will spread on the surface indicating good wetting. If water is used a small contact angle indicates a hydrophilic surface. Conversely, a large water contact angle indicates that the drop remains intact and

beads up, which is typical of a hydrophobic surface. The relationship between contact angle and surface tension/energy is illustrated in **Figure 3.11**.

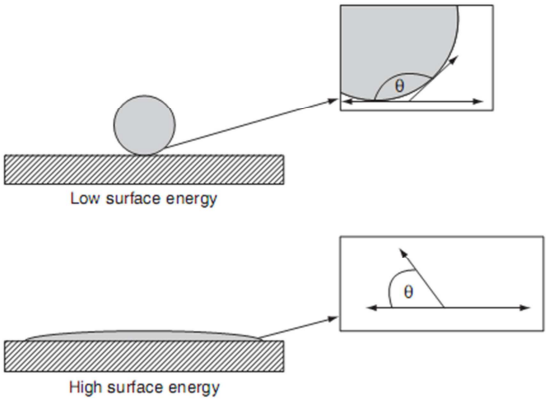

Figure 3.11: Schematic showing relationship between surface energy and contact angle (Goss, 2010).

When the contact angle is low, the surface tension or surface energy of the solid is typically higher than that of the liquid and in order to reduce the interfacial free energy the drop spreads and covers the surface (Hansen, 2000). Conversely for a high contact angle, the surface energy of the solid is typically lower than the liquid, and the drop will remain intact on the surface.

Some of the commonly used methods to determine contact angle include static sessile drop method; dynamic sessile drop method, and dynamic Wilhelmy plate method. In this study the static sessile drop method was used and the contact angle was measured using a contact angle goniometer, and a high-resolution camera was used to capture the image and the contact angle was determined using the DSA 100 software which is based on specific mathematical models.

3.5 DSC

Differential scanning calorimetry (DSC) is a technique used to measure the change in enthalpy (ΔH) or heat flux when a substance undergoes either a physical or a chemical change (Ehrenstein et al., 2004). Enthalpy refers to the amount of heat that is either absorbed or released. Thermal transitions such as melting, evaporation or glass transition are endothermic processes that increase ΔH, while crystallisation,

progressive curing and decomposition are examples of exothermic reactions which are known to decrease ΔH (Ehrenstein et al., 2004).

ΔH is a function of the specific heat capacity (C_p) of a material and change in temperature (dT) as given by **Equation 3.9**.

$$\Delta H = \int C_p . dT \qquad \text{(Eq 3.9)}$$

C_p refers to the amount of energy required to increase the temperature of 1 g of a substance by 1 ℃ at constant pressure (Ehrenstein et al., 2004). Since C_p cannot be easily determined, ΔH is measured by measuring the displacement of heat flux from the baseline. Heat flux $(\dot{Q})$ is the quantity of heat transferred per unit time and mass (m) and is given by Equation 3.10 (Ehrenstein et al., 2004).

$$\frac{\dot{Q}}{m} = v . C_p \qquad \text{(Eq. 3.10)}$$

Where $(\dot{Q})$, m, and v, is the heat flux; mass of the sample; and heating rate respectively.

The principle is based on measuring the difference in heat flow required to keep the sample at the same temperature as the reference (blank pan). During a melting process, the sample absorbs heat (endothermic) as it undergoes melting; hence more heat is required to flow to the sample than the reference to increase their temperature at the same rate. Alternatively during cooling less heat is required, as the material crystallises (exothermic). By measuring this difference in heat flow, the amount of heat absorbed (during heating/melting), or released (during cooling/crystallisation) by the sample can be determined. Both sample and reference (empty pan) are maintained at the same temperature throughout the cycle. The first 10-20 ℃ of the heating cycle compensates for the difference in the sample and reference pans, and transitions in this area are not representative of the sample. Shifts in the melting peak maximum can occur due to the weight of the sample or heating rate, therefore the onset of melting is typically reported.

From the melting and crystallisation peaks, ΔH is calculated as the area under the peak from the peak onset to end-set temperature. The area under the melting peak is

referred to as the heat of fusion ΔH_f which is used to determine the crystallinity of the material.

Two DSC methods are available for measuring heat flux, i.e. Heat flux DSC and power-compensation DSC. For the former, the reference and sample pans are heated together in the same furnace, while for the latter two furnaces are used. In this study a heat flux DSC Q2000 was used. The DSC Q2000 contains the Tzero™ technology, which contains a 3rd thermocouple in the heat flux plate to more accurately account for temperature gradients (Ehrenstein et al., 2004). Tzero™ improves the linearity of the baseline, hence providing more accurate evaluation compared to conventional heat flux DSC's.

3.6 Rheometer

A rheometer is an instrument which is used to measure the rheological properties of a material. Rheology refers to the flow of matter, primarily in the liquid state, but it can also be used to characterise 'soft solids' (e.g. gels, pastes) and/or solids which respond with plastic flow (Wikipedia; 2012c).

In this study a dynamic rheometer was used to characterise the viscoelastic behaviour of materials. An ideally elastic material can be described by Hookes law whereby strain is directly proportional to the applied shear stress and complete recovery of the strain occurs once the applied stress is removed (e.g. rubber) (RheoTec, 2012). Conversely for an ideal viscous material, the constant shear stress leads to a strain which increases linearly over time. If the stress is removed the strain at a particular time will be maintained. However a viscoelastic material displays both elastic and viscous strain whereby partial recovery of the elastic strain is observed while the viscous strain is maintained (RheoTec, 2012). Cross-linked hydrogels display viscoelastic properties.

A parallel-plate model can be used to illustrate the principal of rheology (**Figure 3.12**). The material is placed between the plates whereby the bottom plate is fixed while the top plate is moved with a shear stress and strain.

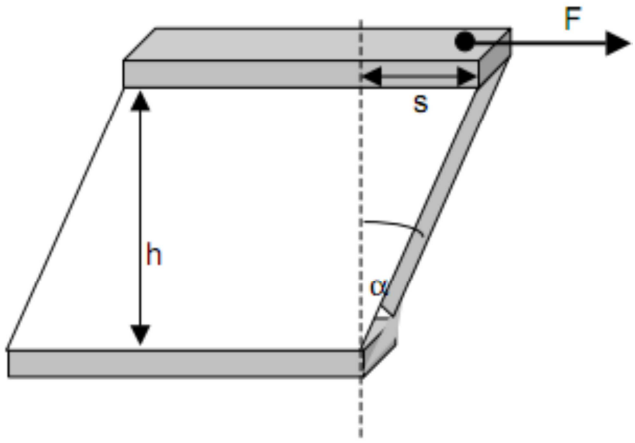

Figure 3.12: Illustration of principal of rheology using parallel-plate model (RheoTec, 2012).

The shear stress (τ) and strain (γ) is described by **Equations 3.11-3.12**.

$$\tau = \frac{F}{A} \quad \text{(Eq 3.11)}$$

$$\gamma = \frac{s}{h} = \tan\alpha \quad \text{(Eq 3.12)}$$

Where F is the applied force, A is the surface area of the plates, s is the distance of displacement, and h is the height between the plates. The complex viscosity of the material (η*) can be determined from τ and shear rate (ẏ) as follows:

$$\eta^* = \frac{\tau}{\dot{y}} \quad \text{(Eq 3.13)}$$

In an ideally elastic material the shear modulus (G) which describes the stiffness or strength of the material is determined as follows:

$$G = \frac{\tau}{\gamma} \quad \text{(Eq 3.14)}$$

However in a viscoelastic material the dynamic complex modulus (G*) is composed of the storage modulus (G′) and loss modulus (G″) as follows: (Anseth et al., 1996):

$$G^* = G' + iG'' \quad \text{(Eq 3.15)}$$

Where G′ is the real (also elastic or storage) modulus and iG″ refers to the imaginary (also viscous or loss) modulus (Anseth et al., 1996). G′ refers to the quantity of energy reversibly stored in the material which is recoverable while G″ refers to the quantity of energy given off or lost. Finally the ratio of G″: G′ describes the damping or dissipation factor (tan δ) (Anseth et al., 1996) (**Equation 3.16**).

$$\text{Tan } \delta = \frac{G''}{G'} \qquad \text{(Eq 3.16)}$$

Tan δ measures the ratio of the energy dissipated as heat to the maximum energy stored in the material during one cycle of oscillation (Anseth et al., 1996).

3.7 References

Anseth KS, Bowman CN, Brannon-Peppas, L. 1996. Review mechanical properties of hydrogels and their experimental determination. Biomaterials 17: 1647-1657.

Birkholz M. 2006. Principles of X-ray diffraction. Thin film analysis by X-ray scattering ISBN: 3-527-31052-5, WILEY-VCH Verlag GmbH & Co. KGaA, Weinheim,

Bovet C, Barron AR. 2009. EPR Spectroscopy: An Overview, http://cnx.org/content/m22370/latest/, Date accessed: 16 August 2012.

Coates J. 2000. Interpretation of infrared spectra, a practical approach. Meyers RA, editor. Chichester: JohnWiley & Sons Ltd. 10815–10837

Ehrenstein GW, Riedel G, Trawiel P. 2004. Thermal analysis of plastics - theory and practice: Hanser Gardner Publications, Inc. 1-26.

Goss B. 2010. Practical guide to adhesive bonding of small engineering plastic and rubber parts: iSmithers Rapra Publishing. 194.

Hansen CM. 2000. Hansen Solubility Parameters : A users handbook: CRC Press LLC. 208.

Philips Electron Optics. 1996. Environmental scanning electron microscope : An introduction to ESEM. Eindhover: Robert Johnson Associates.

RheoTec. Introduction to rheology. Messtechnik GmbH, Ottendorf-Okrilla 2.1E:1-48. http://www.dongjins.com/service/file/Introduction%20to%20rheology, date accessed: 20 August 2012.

Skoog DA, West DM, Holler FJ. 1996. Fundamentals of analytical chemistry: Saunders College Publishing.

Simovič D. 2004. Introduction to the technique of Electron Spin Resonance (ESR) Spectroscopy, Physics Laboratory Course, Available on-line: www. phys. ethz. ch /phys /students /bachelor /vp/VP-Expliste/ESR.pdf, Date accessed: 02 August 2012.

Torres DE. 2006. X-Ray Photoelectron Spectroscopy (XPS), http: //nanohub.org /resources /2109.

Wikipedia. 2012a. Electromagnetic spectrum; http://en.wikipedia.org/wiki/File:Electromagnetic-Spectrum.png. Date accessed 02 August 2012.

Wikipedia. 2012b. Scanning electron microscope; http://en.wikipedia.org/wiki/Scanning_electron_microscope. Date accessed 02 August 2012

Wikipedia. 2012c. Rheology; http://en.wikipedia.org/wiki/Rheology. Date accessed 03 August 2012

Wikipedia. 2012d. X-ray crystallography; http://en.wikipedia.org/wiki/Xray_ crystallography. Date accessed 21 August 2012.

Wikipedia. 2012e. X-ray scattering techniques; http://en.wikipedia.org/wiki/X ray_diffraction. Date accessed 21 August 2012.